AIAA 2000-4584
Application Of Large-Angle Data For Flight Simulation

Edward G. Dickes
John N. Ralston
Bihrle Applied Research Inc.
Hampton, VA

Ken Lawson
Naval Air Systems Command
Patuxent River, MD

AIAA Modeling and Simulation Conference and Exhibit
14-17 August 2000 / Denver, Colorado

APPLICATION OF LARGE-ANGLE DATA FOR FLIGHT SIMULATION

Edward G. Dickes*, John N. Ralston†
Bihrle Applied Research, Inc.
18 Research Drive, Hampton, Virginia 23666
Ken P. Lawson‡
Naval Air Systems Command
Patuxent River, Maryland 20670

Abstract

Large-angle static and dynamic test data were measured for a scale model of the U.S. Navy F-18E/F. Large-angle-of-attack tests were conducted from +90° to +180°and from -90° to -180°. Large-angle-of-sideslip tests were conducted through 90° from -90° to +90° angle of attack. The baseline configuration for these tests consisted of 34° leading-edge flaps, 4° trailing-edge flaps and +2°/+2° ailerons, with the LEX Vent closed.

Aeromodel increments were generated with the extreme angle of attack and sideslip data for the Boeing/Navy F-18E/F aerodynamic simulation database, and were provided as additional tables to extend the current simulation model's coverage.

The application of this large-angle database for flight simulation was successfully demonstrated by the significant improvement in flight correlation and feasibility for the correct modeling of this flight regime for this and other future aircraft.

Introduction

The U.S. Navy, in support of F/A-18E/F Super Hornet EMD flight testing, has sought to continually refine and update their simulation database to provide the highest fidelity engineering simulation of the configuration. As part of the review of the flight motions versus the coverage of the existing simulation database, it has been observed that the post-stall motions of this airplane frequently exceed the table limits of the simulation. The ability of the simulation to properly model the subsequent motions and their recovery to normal flight is impacted on how the simulation handles these off-table excursions. Further, the Naval Air Systems Command has expressed an interest in understanding more about the high angle-of-attack static and dynamic characteristics of their aircraft configurations. As a result, the testing of the F/A-18E/F at extreme angles of attack and sideslip, at static and dynamic test conditions, was undertaken to collect the data necessary to extend the range of the existing simulation, as well as to provide insight about the configuration's characteristics at these conditions.

Large-angle static and dynamic test data were measured for the U.S. Navy F/A-18E/F configuration using a 1/10-scale model mounted on the rotary balance rig in the NASA Langley Research Center 20-Foot Vertical Wind Tunnel (Reference 1), modified to allow a wide range of angle of attack and sideslip combinations (e.g., figure 1). Pertinent aerodynamic effects were extracted from these data and assembled into table form aeromodel increments for use in the Boeing/Navy F/A-18E/F simulation as configured from the February 1998 data release. While more recent aeromodel releases have occurred, it is understood that the most current database has not changed at the table extremes.

Nomenclature

b	wing span, ft
$\bar{c}$	mean aerodynamic chord, ft
C_A	axial-force coefficient, Axial force/ $\bar{q}$ S
C_N	normal-force coefficient, Normal force/ $\bar{q}$ S
C_Y	side-force coefficient, Side force/ $\bar{q}$ S
C_l	rolling-moment coefficient, Rolling moment/ $\bar{q}$ Sb
C_m	pitching-moment coefficient, Pitching moment/ $\bar{q}$ S $\bar{c}$
C_n	yawing-moment coefficient, Yawing moment/ $\bar{q}$ Sb
p, q, r	roll, pitch, and yaw body-axis rates, deg/sec
$\bar{q}$	free-stream dynamic pressure, lb/ft^2
S	reference area, ft^2
V	free-stream velocity, ft/sec
α	angle of attack, deg
β	angle of sideslip, deg

---

* Senior Aerospace Engineer, Senior Member AIAA
† Engineering Manager
‡ Engineer, Member AIAA

Ω rotation rate, rad/sec

$\Omega b/2V$ nondimensionalized wind-axis rotation rate, positive for clockwise spin

δ_a aileron deflection, ($\delta_{a\ left}$ - $\delta_{a\ right}$), deg

δ_h horizontal tail deflection, + TED, deg

δ_{lef} leading-edge flap deflection, + LED, deg

δ_{tef} trailing-edge flap deflection, + TED, deg

δ_r rudder deflection, + TEL, deg

Discussion of Data

The following discussion reviews selected results from the extensive test matrix. This test program was devised in order to augment and extend test data collected earlier in the program, and as a result, coverage of complete angle of attack and sideslip conditions was based on earlier data availability as well as test rig limitations.

Longitudinal Characteristics

The effect of large angles of attack on the normal force and pitching moment are presented in figures 2 and 3 respectively with neutral and full horizontal tail deflections. As seen in the figure 2, the vehicle's normal force characteristics exhibit a relatively constant coefficient value following both upright and inverted stall through approximately ±120° angle of attack, but decreases rapidly at angles of attack beyond. The pitch characteristics maintain the stable slope seen at 90° angle of attack up through the same ±120° angle of attack point, but beyond these conditions the stability goes from neutral to highly unstable above 150° angle of attack. These data would suggest that for this configuration, the extrapolation of the longitudinal characteristics from 90° to 120° would be a reasonable approximation of these data.

The effect of the horizontal deflection shows that for the most part, the effect of control deflection is constrained to below 90° angle of attack. Additional pitch control (with a slight normal effectiveness as well) is derived as the horizontal tails regain limited effectiveness as they develop lift as a forward control surface at approximately ±145° angle of attack.

The effect varying sideslip to ±90° is shown in figure 4 for selected angles of attack. As seen in these data, sideslip variation has a pronounced non-linear effect on the pitch characteristics for all the angles of attack shown. At low angles of attack, sideslip has a limited nose up effect until very high sideslip conditions are reached. Even at 30° angle of attack, the effect of sideslip remains nose down until sideslip is greater than 45°. As angle of attack is increased further, the magnitude of the sideslip angle at which the transition from nose up to nose down pitch decreases, such that by 70°angle of attack, the configuration exhibits nose up pitching moments for any sideslip condition. As seen in these plots, extreme sideslip excursions can result in significant pitch effects.

The variation of pitching moment with sideslip and rotation for large angles of attack is presented in Figure 5. As shown, the pitching moment characteristics at zero sideslip do not vary significantly with rotation throughout most of the high angle-of-attack range, similar to those characteristics seen over the 0° to 90° angle-of-attack range. In the 135° to 145° angle-of-attack region, the pitching moment values become more nose down at the higher rotation rates. The pitching moment vs. $\Omega b/2V$ curves are basically symmetrical for clockwise and counter-clockwise rotations at 0° sideslip angle. At these high angles of attack, the basic rotational characteristics at 0° sideslip angle are essentially unaltered at low sideslip angles. Larger sideslip angles generally skew these curves, resulting in a nose-down increment when the sign of the sideslip angle and rotation rate are the same and, conversely, resulting in a nose-up increment when the signs of sideslip and rotation rate are opposite. The most pronounced effects occur at the highest sideslip angle tested. These effects of sideslip angle on the rotational pitching moment characteristics are typical to those observed over the 0° to 90° angle-of-attack range for the F/A-18E/F and other aircraft configurations, although the lower sideslip angles provide more of an influence on the rotational characteristics of the F/A-18E/F within the 0° to 90° angle-of-attack range.

Lateral Characteristics

The effect of sideslip on the static roll characteristics is presented in figure 6 for selected angles of attack. As seen in figure 6, the effect of sideslip at extreme sideslip angles can have a dramatic effect on the basic stability characteristics of the airplane. At very low angles of attack, little lateral stability is evidenced at any sideslip angle. As angle of attack is increased to near stall (30°), however, lateral stability increases through 45°of sideslip, followed by a gradual transition to lateral instability. By 45° angle of attack the configuration remains very stable with a linear variation with sideslip that abruptly changes to similar levels of instability at 45° of sideslip. The sideslip at which this transition occurs increases as angle of attack increases, up to 60° sideslip by 70°angle of attack.

The effect of aileron through an angle of attack range of ±180° is presented in figure 7 for rolling moment. Limited roll authority persists through

±90° angle of attack, with an abrupt reversal of control power at approximately ±160° angle of attack.

The rotational rolling moment characteristics at high angles of attack as a function of sideslip are presented in Figure 8. At 90° angle of attack, the rolling moments at 0° sideslip angle are slightly propelling, a characteristic typical of most aircraft. This propelling tendency gradually increases with increasing angle of attack through 125° angle of attack, with sideslip exhibiting little influence on the rotational variation. By 165° angle of attack, rolling moments are once again, only slightly propelling at the higher rotation rates, with more pronounced sideslip effects on the rotational characteristics. At the extreme angles of attack above 165°, rotation about the velocity vector produces large unstable body-axis rolling moments, and an increase in the effect of sideslip on damping characteristics.

Directional Characteristics

The effect of sideslip on the yawing moment is shown in figure 9. The influence of sideslip is particularly non-linear in the pre stall angles of attack for this airplane. At low angles of attack the airplane initially exhibits directionally stability that reverses to instability by 20° of sideslip. This unstable trend reverses again at very high sideslip angles. As the angle of attack increases, the region of stability decreases, with substantial unstable directional characteristics persisting to high sideslip. The angle of sideslip at which the directional characteristics reverse to stable slopes decreases as angle of attack increases. This is particularly evident at 40° angle of attack, where significant directional instability is evident through 30° of sideslip, followed by recovery of stable directional slopes. The variation of these transition points illustrates the difficulty in building an appropriate off table approximation (held or extrapolated) for tables fixed at a particular lower sideslip value.

Figure 10 illustrates the variation of rudder control power versus ±180° angle of attack. While rudder power is significantly diminished for upright angles of attack by 60° until achieving limited power when facing into the flow at very high angles of attack, inverted rudder power persists past -90° angle of attack. Also note the presence of forebody induced asymmetric yaw characteristics at both ± 55° to 60° angle of attack at zero sideslip.

The influence of sideslip angle and rotation on the high angle-of-attack yawing moment characteristics is presented in Figure 11. The basic aircraft at zero sideslip is remains damped in yaw throughout the 90° to 180° angle-of-attack region. A gradual reduction in yaw damping is observed as the angle of attack increases. In general, sideslip has no effect on the rotational characteristics in yaw until high sideslip angles are achieved.

Data Mechanization and Simulation Results

The evaluation of the large angle wind tunnel test data's impact on an existing simulation's ability to model aerodynamic behavior at extreme angle of attack conditions was a major component of this effort consequently, the development of the test data into suitable simulation model tables was undertaken. These tables were then mechanized in an existing engineering simulation to enable simulation review and comparison with existing flight test data that exhibited excursions into this flight regime.

The integration of the new wind tunnel data with the existing simulation presented several challenges. The existing model structure inherent in the F/A-18E/F simulation adds the high angle of attack and sideslip data as an increment off of the low angle of attack model (α<40°, β<30°). Consequently, the development of additional incremental effects would have added significantly to an already complex model build up. In order to minimize the work required to add the substantial large-angle data to the existing model, these database extensions were included in the model structure as stand alone tables, with the full coefficient effect inherent in the tables. This modeling required the alignment of the individual coefficients for the baseline configuration, as well as the incremental effects of controls and rotational data for smooth transitioning. In order to arrive at a comparable simulation value to align the new model data with, the simulation was "driven" with state values at the same conditions and test points as the wind tunnel data. The resulting 'virtual wind-tunnel' output was collected into comparable tables that could be evaluated against the new wind tunnel data.

The plotted data were organized as a comparison of the high sideslip (45°) overlap comparisons for the basic airplane, as well as the effects of horizontal tail and rudder, followed by the angle of attack overlap comparisons at ±90°. In general, these results showed good agreement between the simulation and the new test data at these conditions, and the adjustment of the new tables to align with the existing simulation results required only small changes to the new tables to arrive at the desired overlap in most cases. There were other conditions that required more significant changes to the test data so that the desired identical data values at the table endpoints were achieved. In these cases, the changes

were propagated further into the new data set. In the case of the high sideslip tables, initially the 45° table values in the new tables were simply replaced with the current simulation output at that sideslip condition. It was felt that in this manner, the seamless transition from the existing simulation to the new data could be accomplished without adding additional incremental effects, and without using a ramping function.

The new model data were constructed as separate data regimes, or cases, that enabled the complete coverage of the angle of attack and sideslip space. Based on the value of angle of attack and sideslip, the model transitioned between the cases as shown in Figure 12. This modeling called for the replacement of the appropriate tables in the original Boeing simulation data reconstruction with the new tables whenever the particular cases occurred. Effectively, as the model excursion went above 45° sideslip, the data that defined the basic airplane characteristics as well as the rudder and horizontal tail effects (the only terms collected during the recent tests in this portion of the envelope), would be replaced in the original Boeing coefficient build-up. This meant that initially all other terms in the build-up would be propagated into the large-angle conditions.

This new model structure was incorporated into the BAR simulation of the F-18E/F using the FEB98 aerodynamic data set and the Version 7.02 flight control (Reference 2). A modification of the dynamic data mechanization method proposed by Kalviste (Reference 3) was used to mechanize the rotary and body axis dynamic data. Several departure and spin flights from recent flight tests that exhibited excursions into extreme angles of attack and sideslip were selected as examples with which to evaluate the effect of the extended model. The flight state variables from these flights were imported into the simulation and used to "OverDrive" the simulation. A flow chart describing the "OverDrive" process is shown in Figure 13. This analog matching technique drives the simulation in a stepwise form using the flight states as inputs to the simulation tables to derive total simulation force and moment output time histories. The resulting simulation moment time histories were compared to those extracted from the flight test data. Several issues became apparent as these comparisons were generated using the original model build up. While the incorporation of the new large-angle data had a significant beneficial effect when compared to flight as the airplane excursions went into the newly modeled regions, terms that were carried from the original model build-up appeared to have an adverse influence on the coefficient comparisons. This was particularly true in the high sideslip excursion case (Case 1 in the diagram shown in Figure 12). Further inspection showed that many of these terms in the original model were not modeled as a function of sideslip and the persistence of their influence into the high sideslip region was deemed inappropriate. As a result, the model cases described above were modified to omit all but the new test data as the model transitioned between the Case 0 (original Boeing model envelope) and Case 1 (high sideslip condition). By transitioning to strictly the high sideslip test data in this fashion, the model correlation in this part of the envelope was significantly improved for the flights examined, as shown in the flight comparisons of Figures 14 through 16.

Examination of the flights used in this evaluation, which included two departures and an upright spin that transitioned inverted, shows a significant improvement over the original model which held table values for off table excursions. While not evaluated in this effort, the effect of extrapolating the off table excursions is expected to yield comparisons at least as dramatic as those shown here, given the wildly fluctuating states that occur as the table look-ups exceed the original table ranges. Another conclusion that can be drawn from these results is that the angle of attack and sideslip are the principal data functionalities at these large-angle conditions, with most other dependencies small in comparison to the large forces and moments generated by these terms. This is evident in the close match between flight and the model during excursions into the Case 1 model region, using a database that is primarily a function of angle of attack and sideslip. Because of this, an evaluation of how the existing model handles some of the other coefficient build-up terms as these extreme angles are approached is recommended.

Concluding Remarks

Large-angle static and dynamic aerodynamic characteristics were measured for a 1/10-scale model of the U.S. Navy F/A-18E/F utilizing the rotary balance test rig in the NASA Langley Research Center 20-Foot Vertical Wind Tunnel. Aeromodel increments of these data have been generated with the extreme angle of attack and sideslip data for the F-18E/F aerodynamic simulation database, and were built as additional simulation tables to extend the current simulation model's coverage.

The existing F-18E/F simulation model has proven to be a highly effective tool for predicting flight response through the majority of the airplane's flight regime. Nevertheless, certain departed conditions exhibit extreme variations in angle of attack and sideslip, well beyond the limits of the simulation database. The integration of the newly

devised data tables enabled the evaluation of this low speed test data at these conditions. Comparison of the flight extracted coefficient data with results predicted from the original simulation and the revised large-angle database showed significant improvement over the original model, which held table values for off-table excursions. It was also seen that angle of attack and sideslip are the principal data functionalities at these large-angle conditions, with most other dependencies small in comparison to the large forces and moments generated by these terms. The significant improvement in the flight correlation realized by including a low-speed static wind tunnel database model of this portion of the envelope illustrates the benefit of modeling the fundamental aerodynamics in this flight regime. Further application of these data for future configurations can play an important role in the a priori identification and suppression of large angle departure motions.

References

1. Dickes, E., Ralston, J. and Kloc, S., "F-18E Large-Angle Testing: Static and Dynamic Characteristics From Rotary Balance Wind Tunnel Test Data and Aeromodel Increments", BAR 99-05, June 1999.
2. Kay, J.,"F-18E/F FEB98AERO Model Rehost Static Check Case Verification Results", BAR 99-07M, July 1999.
3. Kalviste, Juri: Use of Rotary Balance And Forced Oscillation Test Data In A Six Degrees Of Freedom Simulation, AIAA Paper 82-1364, August 1982.

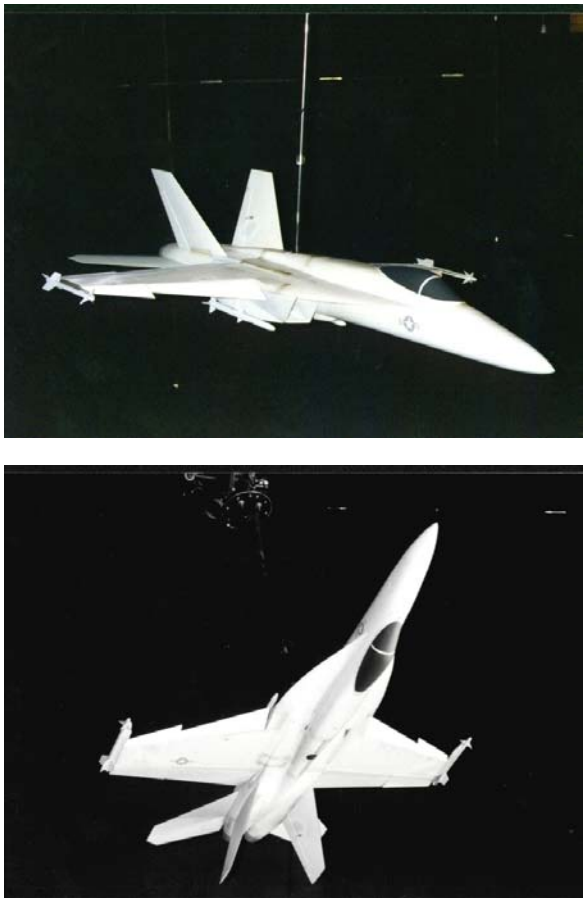

Figure 1. Large-Angle Testing of the F/A-18E/F Model.

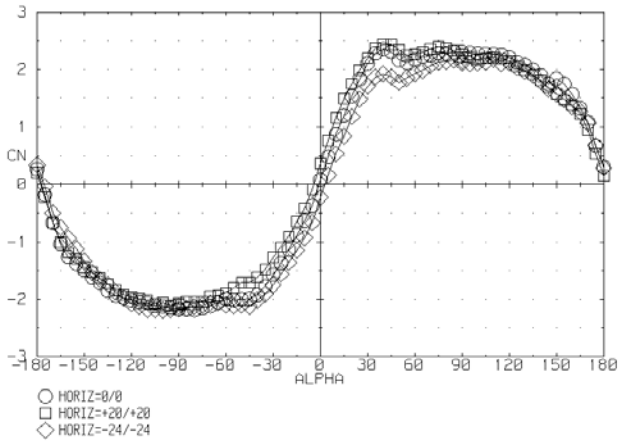

Figure 2. Effect of Angle of Attack and Horizontal Deflection on Normal Force

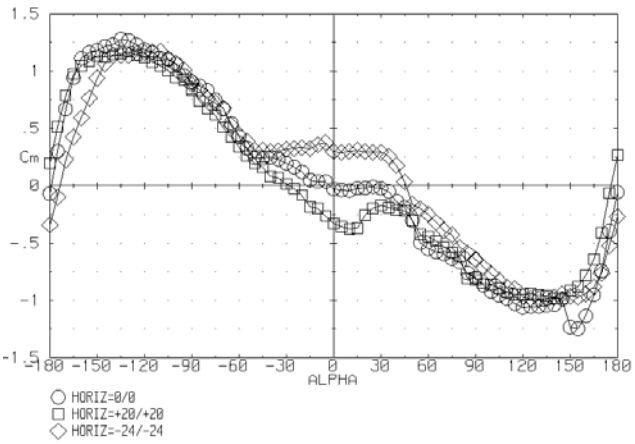

Figure 3. Effect of Angle of Attack and Horizontal Deflection on Pitching Moment

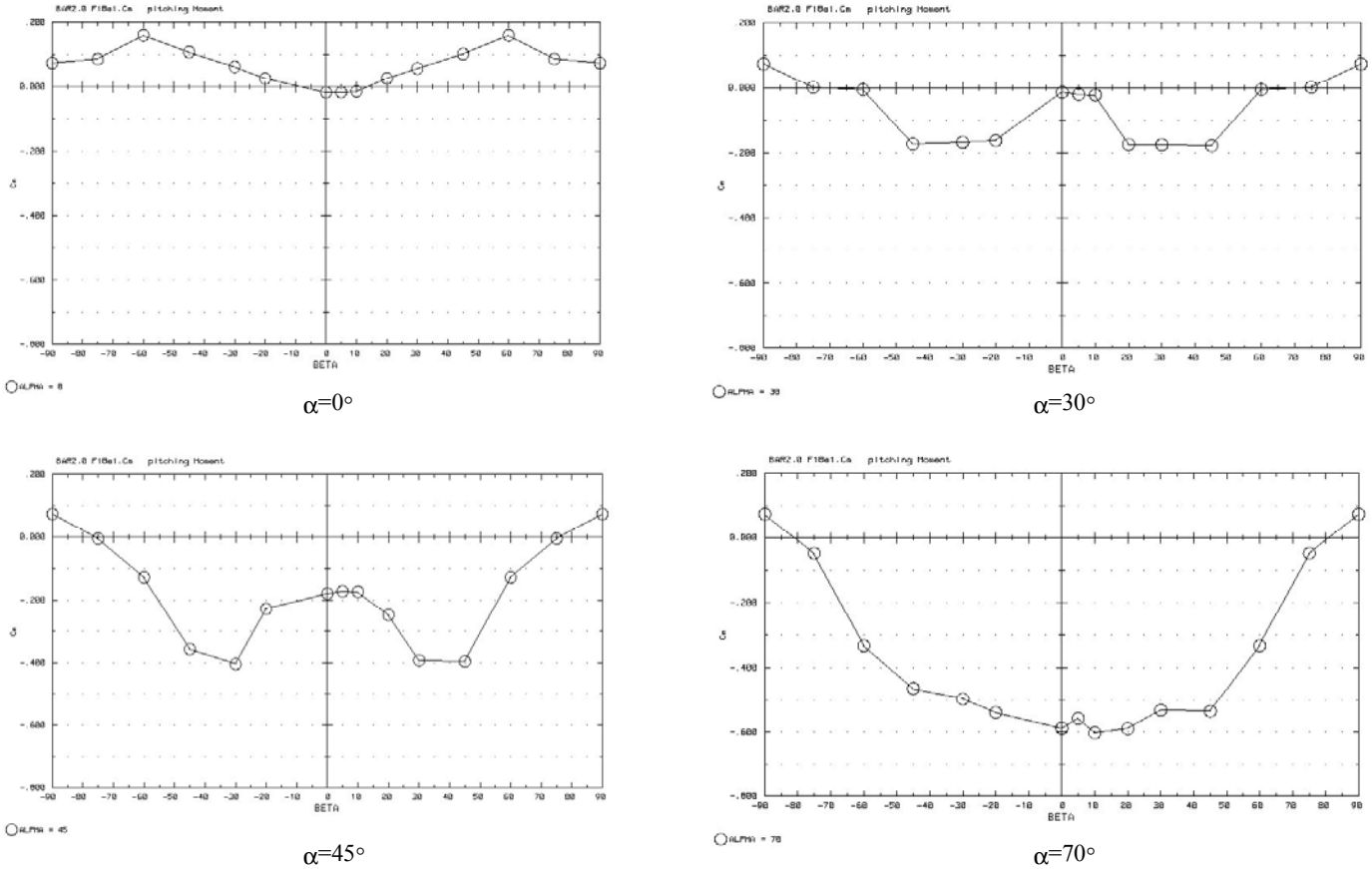

Figure 4. Effect of Sideslip on Pitching Moment

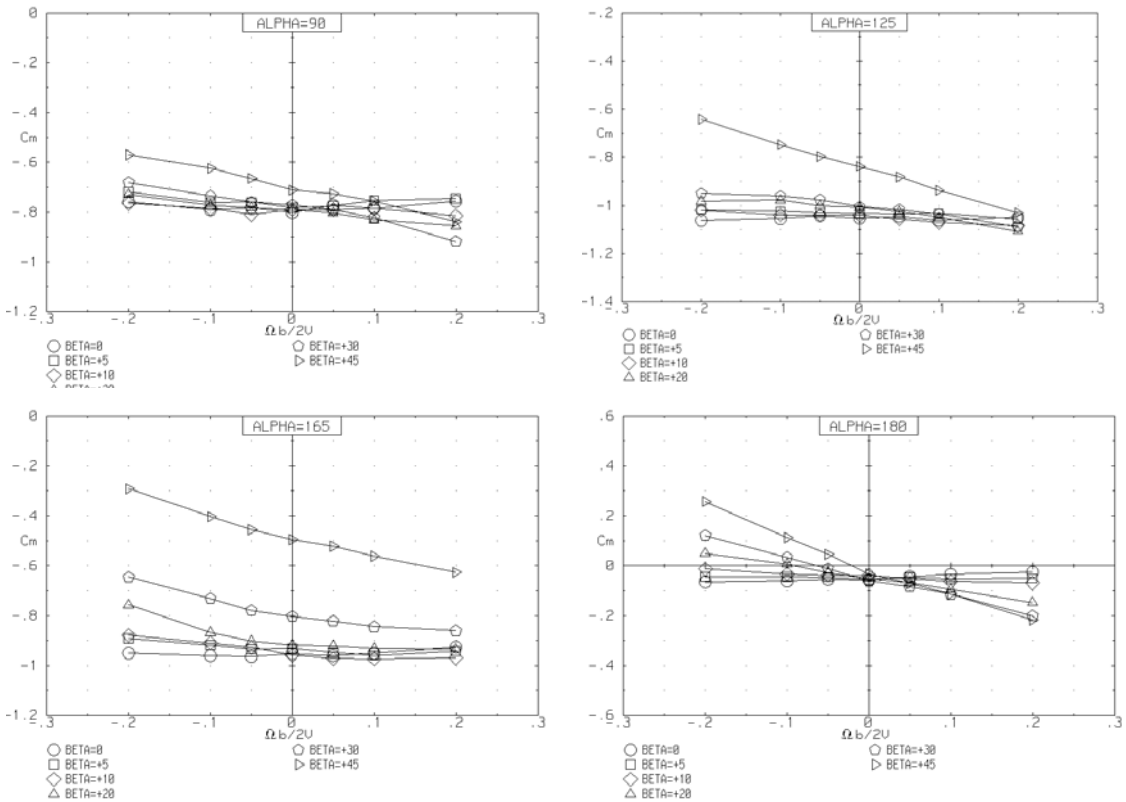

Figure 5. Large-Angle Rotational Pitching-Moment Characteristics

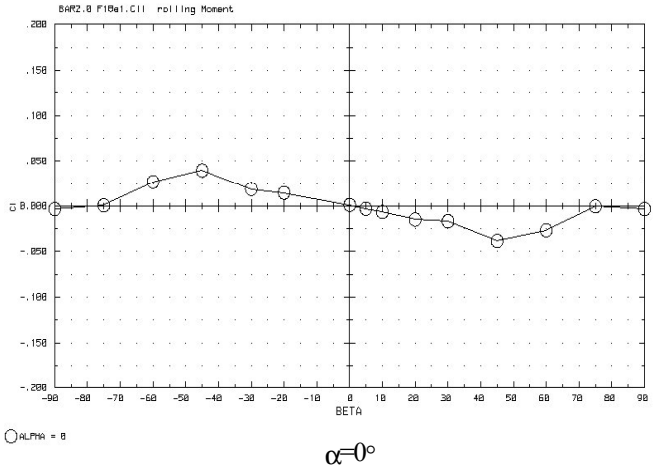

α=0°

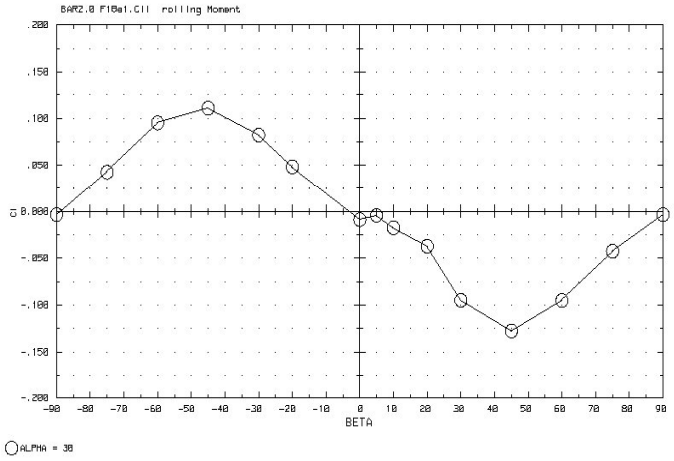

α=30°

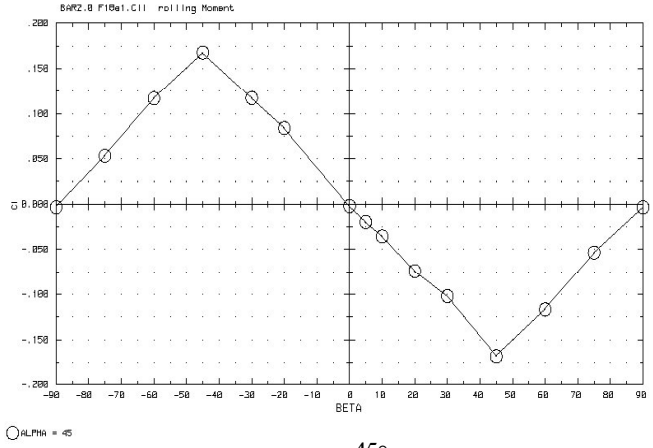

α=45°

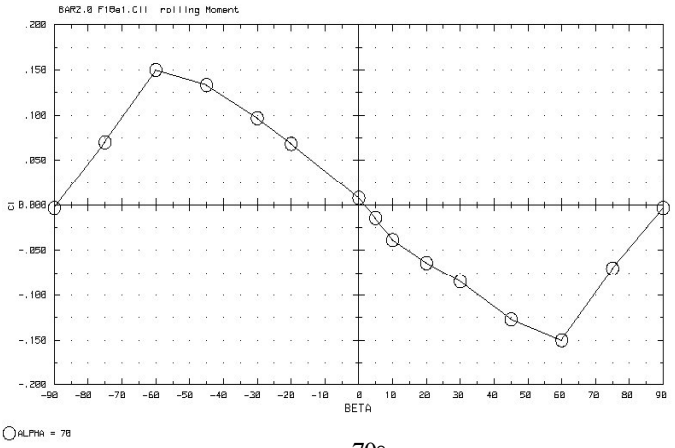

α=70°

Figure 6. Effect of Sideslip on Rolling Moment

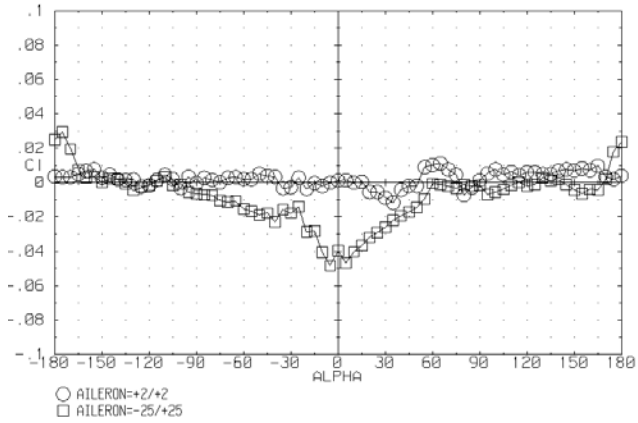

Figure 7. Effect of Aileron Deflection at Large Angles of Attack

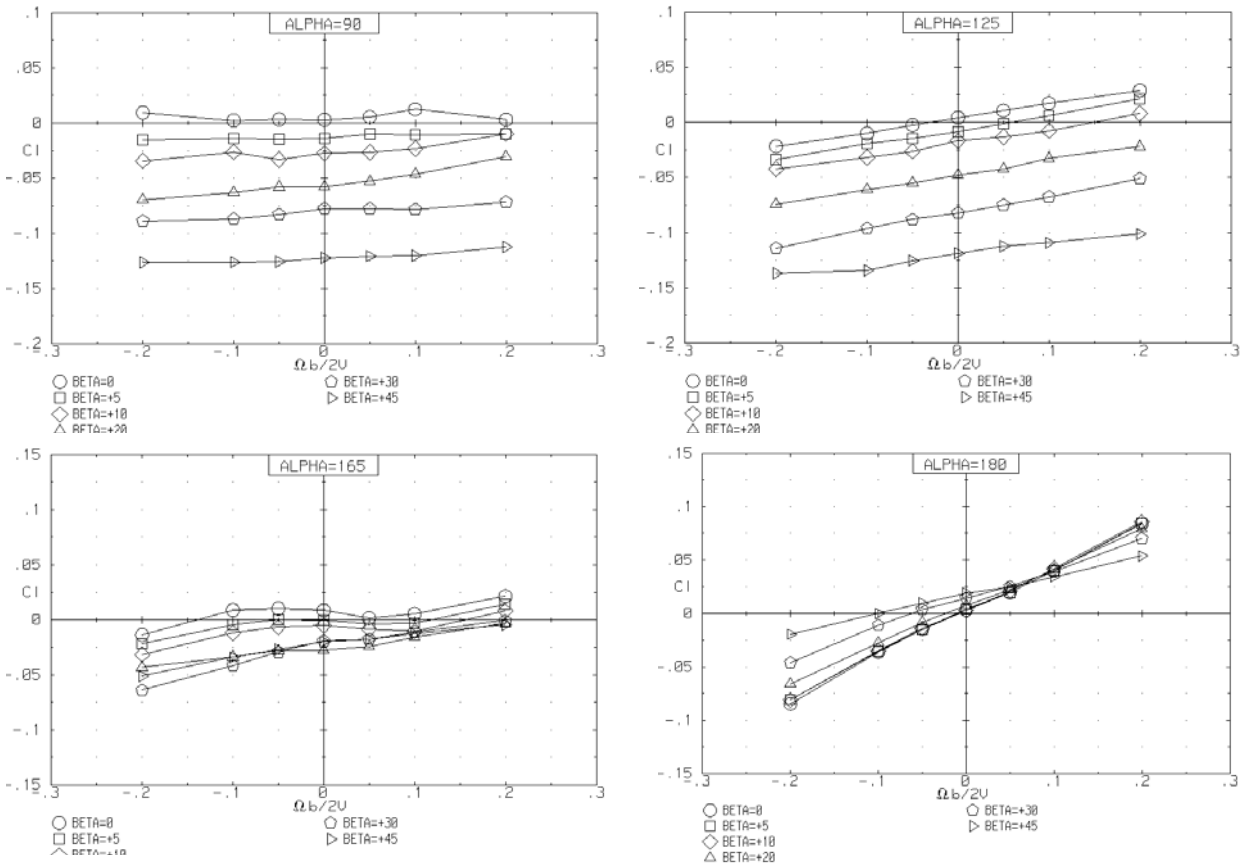

Figure 8. Large-Angle Rotational Rolling-Moment Characteristics

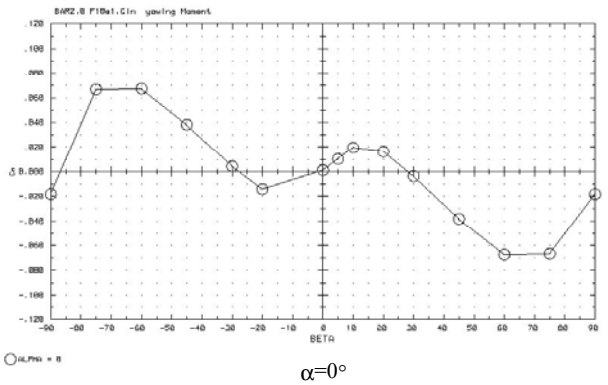

α=0°

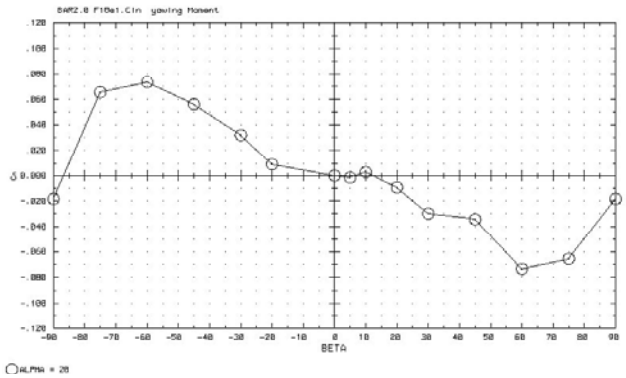

α=20°

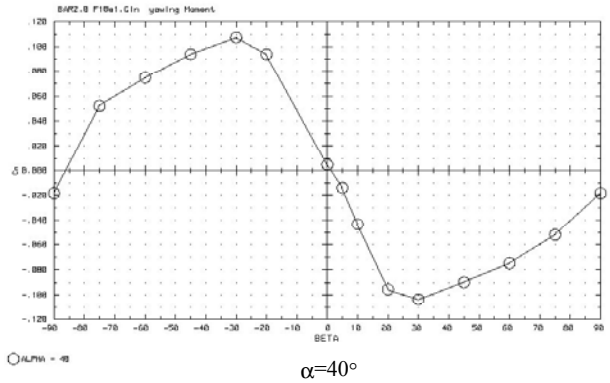

α=40°

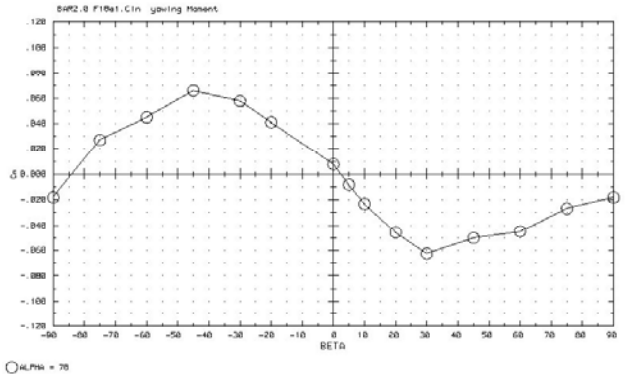

Figure 9. Effect of Sideslip on Yawing Moment

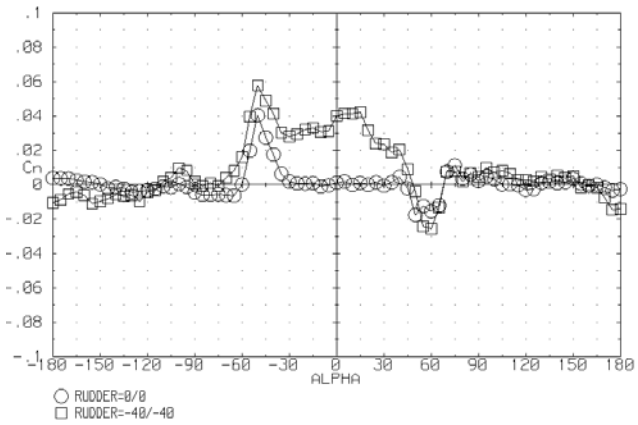

Figure 10. Effect of Rudder Deflection at Large Angles of Attack

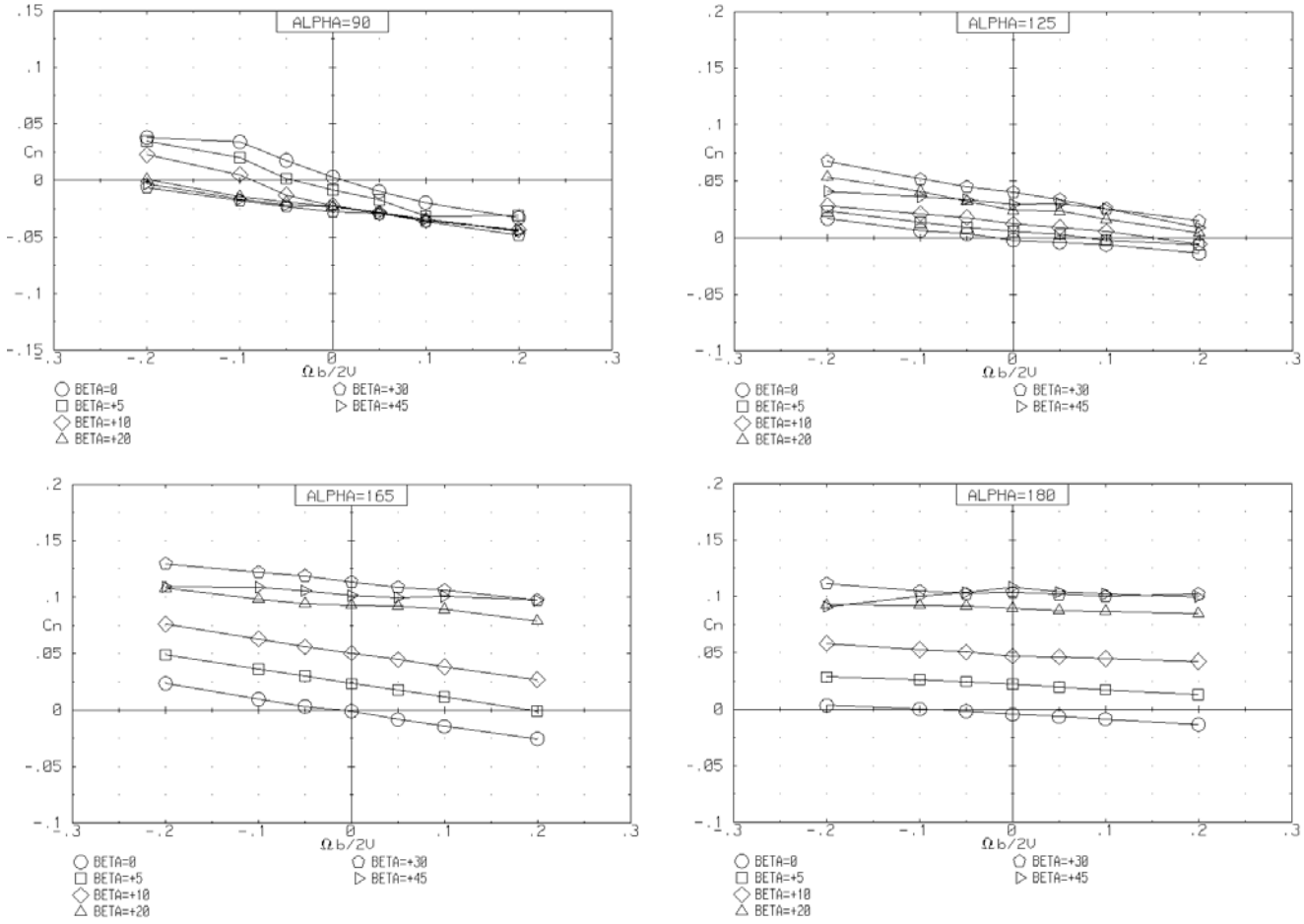

Figure 11. Large-Angle Rotational Yawing-Moment Characteristics

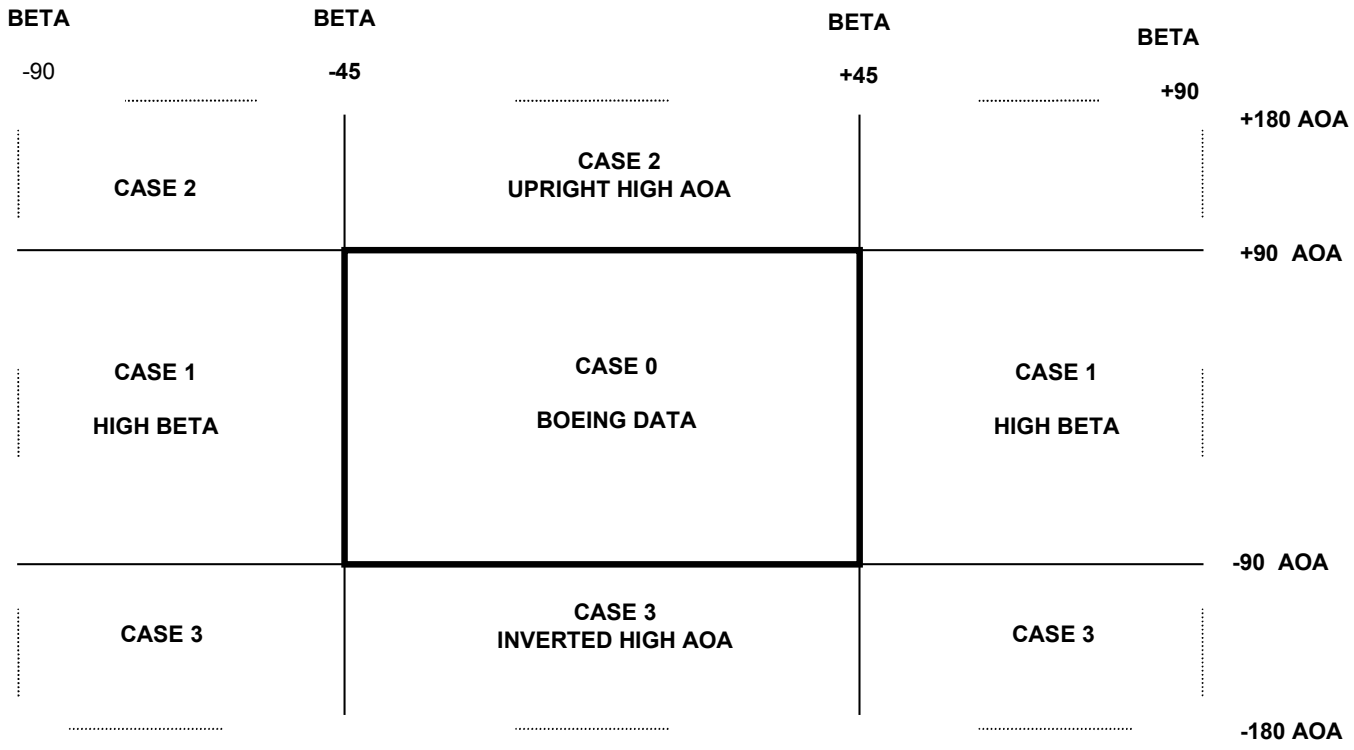

Figure 12. Case Conditions Describing the New Database Extents

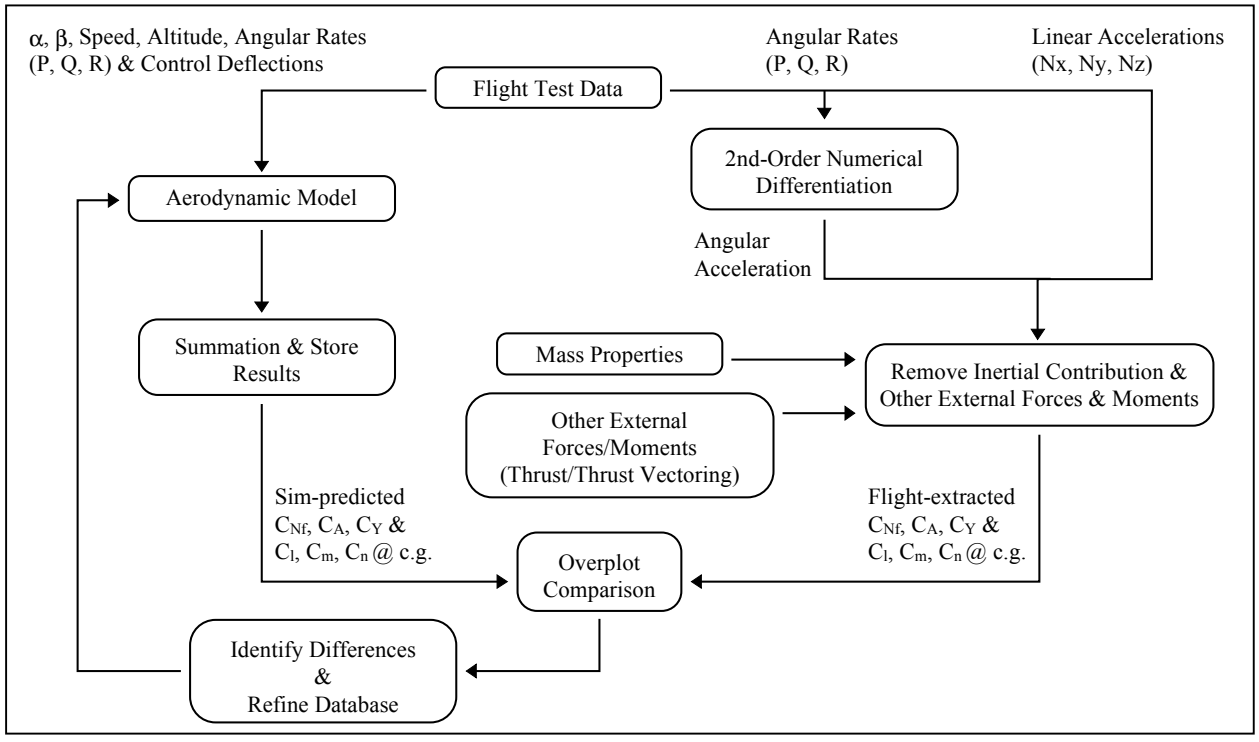

Figure 13. Schematic Of Typical 'OverDrive Technique.

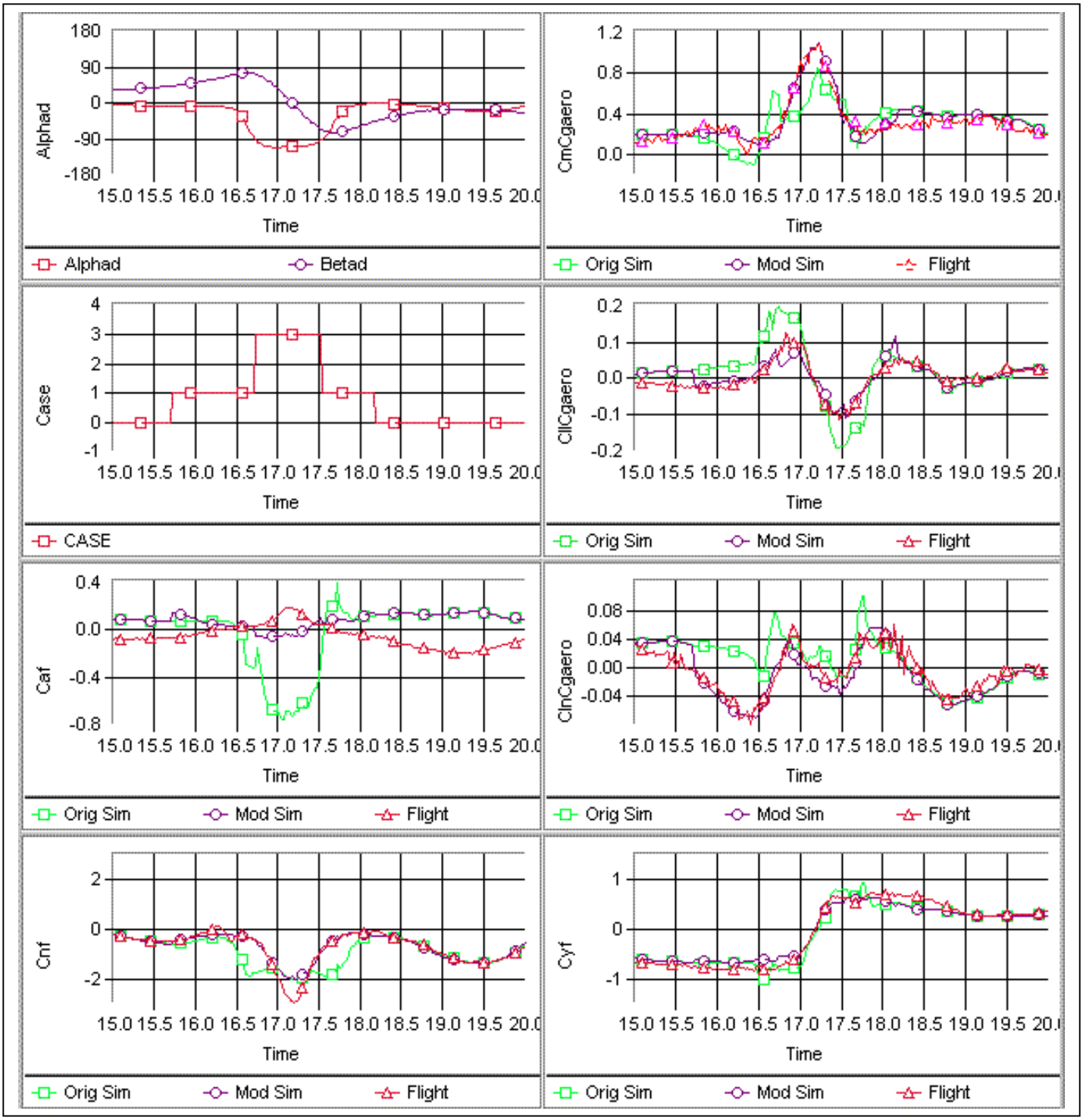

Figure 14.- Flight 231-35 Departure
Comparison Of Flight Extracted Coefficient Data With Results Predicted From The FEB98 Simulation
And Revised Database

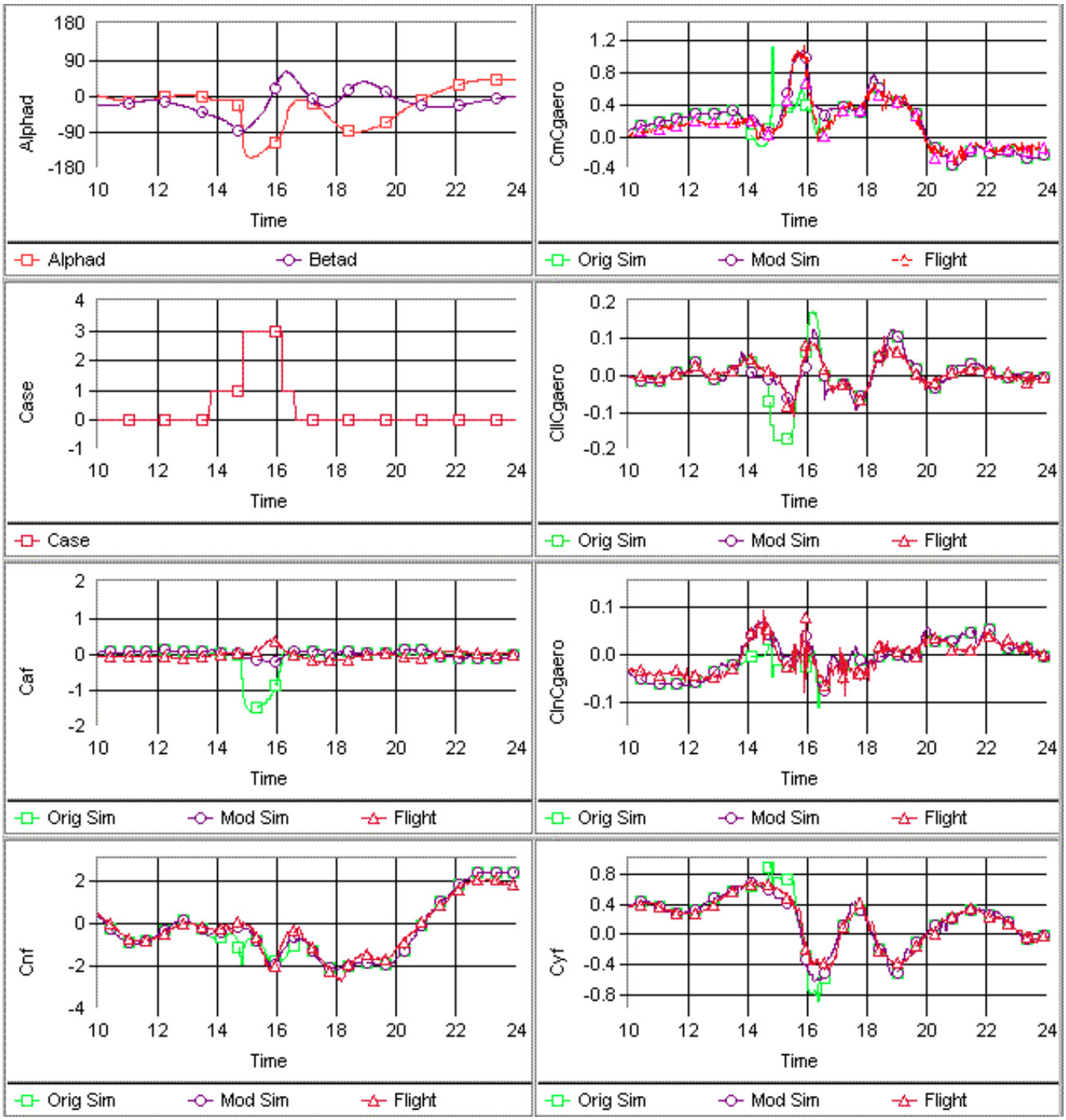

Figure 15.- Flight 230-19 Departure
Longitudinal Comparison Of Flight Extracted Coefficient Data With Results Predicted From The FEB98 Simulation And Revised Database

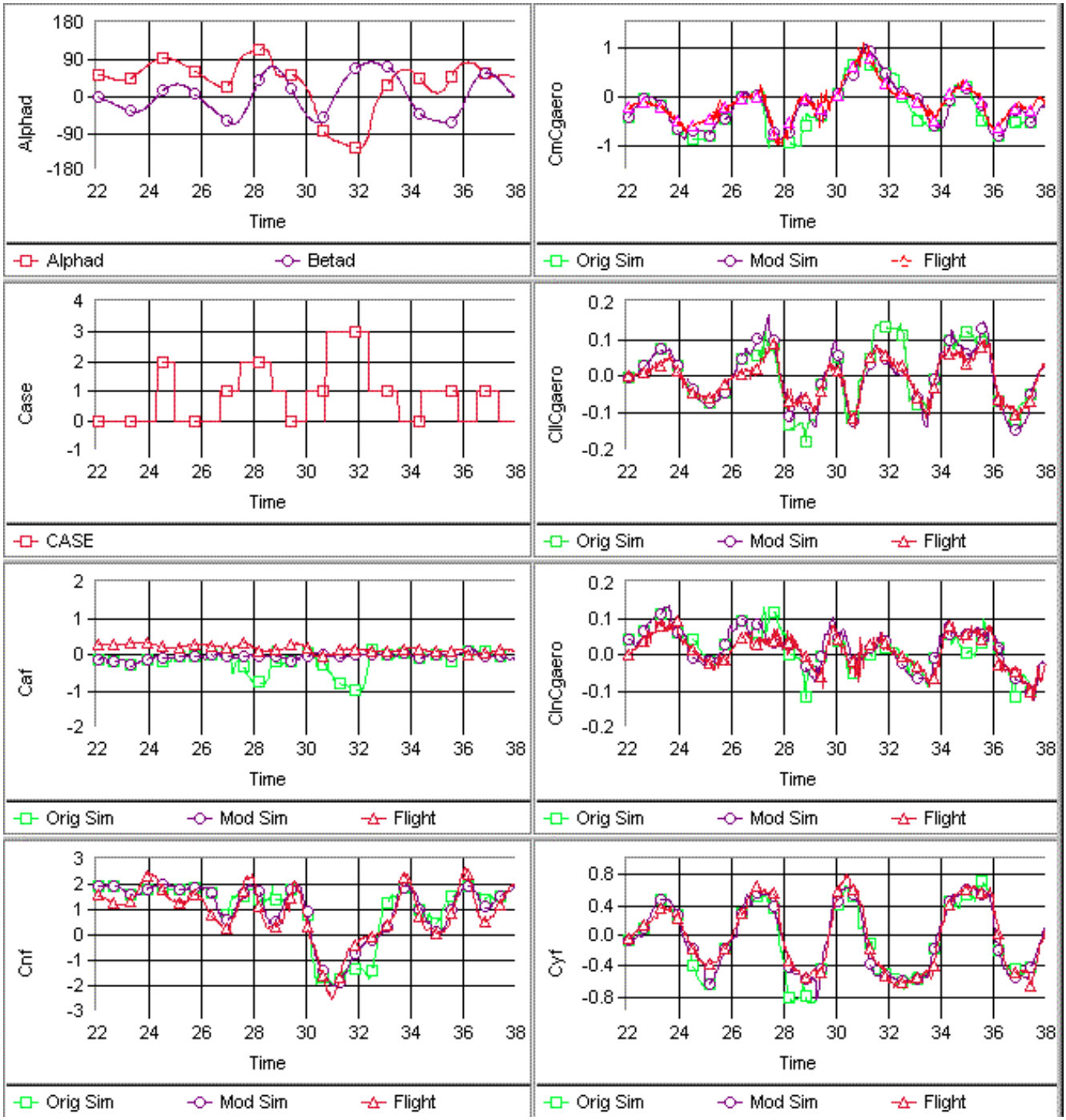

Figure 16.- Flight 234-24 Upright Spin
Comparison Of Flight Extracted Coefficient Data With Results Predicted From The FEB98 Simulation And Revised Database